AIAA JOURNAL
Vol. 36, No. 8, August 1998

Large-Eddy Simulations and Lidar Measurements of Vortex-Pair Breakup in Aircraft Wakes

D. C. Lewellen* and W. S. Lewellen†
West Virginia University, Morgantown, West Virginia 26506-6106
L. R. Poole‡
NASA Langley Research Center, Hampton, Virginia 23681-0001
R. J. DeCoursey§
Science Applications International Corporation, Hampton, Virginia 23666
G. M. Hansen¶
Science and Technology Corporation, Hampton, Virginia 23666
C. A. Hostetler**
NASA Langley Research Center, Hampton, Virginia 23681-0001
and
G. S. Kent††
Science and Technology Corporation, Hampton, Virginia 23666

Results of large-eddy simulations of an aircraft wake are compared with results from ground-based lidar measurements made at NASA Langley Research Center during the Subsonic Assessment Near-Field Interaction Flight Experiment field tests. Brief reviews of the design of the field test for obtaining the evolution of wake dispersion behind a Boeing 737 and of the model developed for simulating such wakes are given. Both the measurements and the simulations concentrate on the period from a few seconds to a few minutes after the wake is generated, during which the essentially two-dimensional vortex pair is broken up into a variety of three-dimensional eddies. The model and experiment show similar distinctive breakup eddies induced by the mutual interactions of the vortices, after perturbation by the atmospheric motions.

I. Introduction

RECENT research on the evolution of aircraft wakes has focused on assessing the impact of increased aircraft traffic on the environment,[1,2] particularly potential effects of exhaust species on ozone levels in the atmosphere and of persistent contrails on the Earth's radiation balance. The extent to which the dynamics and mixing in the aircraft wake at early times, which we consider in this work, may ultimately affect the chemical composition of the wake at late times is largely unknown. A recent extensive review of the dynamics of aircraft trailing vortices by Spalart[3] shows that, in spite of 30 years of research on this topic, many questions remain on how to predict the breakup of the wake vortices.

It is convenient to identify four overlapping regimes in the evolution of an aircraft wake. During the first few seconds, the vorticity distribution from the wing rolls up into a pair of trailing vortices, while the engine exhaust jets mix with the ambient air, largely independent of the roll-up process. The wake dynamics following this roll-up/jet regime are dominated by the interactions of the vortex pair. Typically, in this stage the engine exhaust jets partly wrap into the vortex cores and partly detrain into a buoyant plume; the vortices fall and interact with each other through a mutual induction sinusoidal instability and with any ambient shear that is present, until they finally break up, typically within a few minutes. After vortex breakup, positive buoyancy acquired from the hot engine exhausts and from the vortex pair falling through any ambient stratification can dominate the dynamics until the plume mixes sufficiently with the ambient air, typically within one or two Brunt–Vaisala periods (~10 min). Finally, at later times, the plume dispersion is dominated by the interaction with the ambient atmosphere, via atmospheric turbulence, gravity waves, and shear. In a previous paper,[4] hereafter denoted as LL96, we presented results of large-eddy simulations (LES) focused on the middle two regimes of wake evolution, dominated by the vortex interactions and buoyant plume dynamics. References to some recent LES studies concentrating on the vortex dynamics (addressing the problem wake vortices present to air traffic control) can be found in Spalart's[3] review. Gerz et al.[5] also treat species dispersion in the wake as well as considering the other regimes in the wake decay.

Some of the lidar observations from the Subsonic Assessment Near-Field Interaction Flight Experiment (SNIF) performed at NASA Langley Research Center follow the wake evolution well into the vortex breakup stage in a series of runs in which the aircraft flies directly over the lidar site in a direction parallel to the ambient wind. The design of this experiment is briefly described in Sec. II. The purpose of the present paper is to make comparisons between model simulations and experimental results. This permits a comparison that is more quantitative than the comparison between model and photographs made in LL96 and by Gerz et al.[5] Any model invariably treats only a subset of the physics involved; a favorable comparison with experiment can lend confidence to the assertion that those pieces left out are not of significant importance to the phenomena under study. The basic code and general setup are the same as presented in LL96. As discussed in Sec. III, we attempt to approximate ambient atmospheric conditions as far as they are determined and use initial conditions appropriate for the specific aircraft a few seconds after it has passed. The initial configuration and properties of the vortices and exhaust jets, which are important to the dynamics in our regime of interest, are taken as modifications of the results obtained from the computations of Quackenbush et al.[6,7]

Received Nov. 14, 1997; revision received April 27, 1998; accepted for publication May 5, 1998.

*Research Assistant Professor, Mechanical and Aerospace Engineering Department.
†Research Professor, Mechanical and Aerospace Engineering Department. Member AIAA.
‡Aerosol Research Branch Head, Atmospheric Sciences Division.
§Computer Systems Specialist.
¶Staff Scientist.
**Research Scientist, Aerosol Research Branch.
††Senior Scientist.

II. Experimental Setup

The measurements that we compare to the model data were collected by two ground-based lidars operated by the Aerosol Research Branch (ARB) at NASA Langley Research Center (LaRC).[8] Lidar, an acronym for light detection and ranging, is a time-of-flight remote-sensing technique in which laser pulses are transmitted toward the volume to be sensed and photons that are backscattered from hard or, in this case, distributed targets, i.e., atmospheric aerosols, are collected by a telescope receiver. By measuring the instantaneous strength of the backscattered signal and the time difference between the emission of the laser pulse and the receipt of that signal, a range-resolved, line-of-sight profile of backscatter can be determined. The observations reported in this paper were computed from large sequences of lidar backscatter profiles collected with the intent of determining the spatial distribution of exhaust particulates in the wake of a Boeing 737 (B-737) aircraft. The LaRC Boeing 737-100 Transportation Systems Research Vehicle was used as the source aircraft to generate the wake. This aircraft normally is used for development and testing of advanced flight systems concepts and hardware as part of LaRC's aeronautics mission. The LaRC B-737 is equipped with differential Global Positioning System (GPS) instrumentation and computer-controlled fly-by-wire technology that allows the crew to fly the aircraft along flight paths with accuracies of a few meters. This level of precise positioning was required to provide a controlled experiment from which measured and model data could be compared realistically.

The flight geometry employed to collect the data was one in which the B-737 was flown parallel to the ambient wind at an altitude of 3.20 km with zero flap deflection directly over the ARB lidar site at Langley (lat N 37° 06′ 17.8500″ and long. W 76° 22′ 43.1006″). Immediately after each overpass of the site, the two ground-based lidars began to acquire profiles of backscatter from the B-737 exhaust plume. Because of the parallel-to-wind geometry, the exhaust plume and wake vortices of the B-737 tended to remain over the site as the vortex pair evolved in time. Assuming the exhaust particulates to be adequate tracers of fluid motion, the lidars were able to monitor the uptake of the engine exhaust into the vortex pair and the evolution of the vortex structure. Subsequently collected profiles of backscatter from the entrained exhaust aerosols provide a three-dimensional space-time history of the evolution of the wake vortex pair.

Two lidars were involved in the experiment: the ARB scanning lidar, which has a 14-in.-diam collecting telescope and is capable of scanning in both azimuth and elevation, and the ARB 48-in. lidar, which is a fixed zenith-pointing system with a 48-in.-diam collecting telescope that is capable of greater sensitivity and higher vertical resolution than the scanning lidar. After each B-737 overpass, the scanning lidar acquired two-dimensional profiles of lidar backscatter from the B-737 wake vortex pair by scanning the lidar-sensing volume across the vortex structure in a plane nominally perpendicular to the flight path of the aircraft (see Fig. 1). By repeatedly scanning back and forth across the vortex structure, the scanning lidar was able to record the evolution of the wake structure for as long as the vortex pair remained intact and the exhaust particulates remained at a high enough concentration to provide a distinguishable signal above that from the background atmosphere. The resulting data sets essentially provide a three-dimensional (horizontal, vertical, and temporal) sampling of the vortex structure. In this observational geometry, the 48-in. lidar was able to collect only two-dimensional (vertical and temporal) measurements of the wake structure because of its zenith-only viewing mode. General operational parameters for both lidars used in the SNIF experiments are given in Table 1.

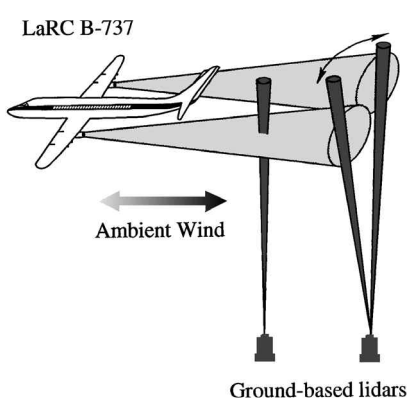

Fig. 1 Observational geometry employed for the ARB scanning lidar during SNIF for parallel-to-wind overflights of the B-737.

Table 1 Relevant parameters of ARB lidars used in SNIF

Parameter	Scanning lidar	48-in. lidar
Wavelengths	1064 nm	532 and 1064 nm
Energy/pulse	500 mJ	500 mJ each wavelength
Telescope area	0.1 m^2	1.13 m^2
Field of view	0.5 mrad	0.5 mrad
Repetition rate	30 pulses/s	20 pulses/s
Scan rate (one pass)	~1 transverse scan/s	——
Vertical resolution	7.5 m	3 m
Effective horizontal resolution	~3 m[a]	2 m[b]

[a]Determined by scan rate, maximum scan angle, repetition rate, and altitude of plume.
[b]Diameter of laser-beam cross section at the altitude of the plume.

III. Model Review and Setup

As discussed in LL96 the LES code developed for this work is derived from an LES code developed primarily for boundary-layer cloud modeling.[9,10] It is a three-dimensional finite difference implementation of the incompressible Navier–Stokes equations in the Boussinesq approximation, second-order accurate in space and time. The subgrid model utilizes a quasiequilibrium, second-order turbulence closure scheme with the maximum subgrid turbulence length scale related to the numerical grid length. It incorporates a piecewise parabolic model algorithm for the advection of temperature and species concentrations. Obtaining adequate resolution is the most fundamental difficulty in these simulations. A grid spacing of a few percent of the wing span or less is required to resolve the trailing vortex cores and the transport of the engine exhausts around and into them. On the other hand, line vortices have a sizable long-range influence on the flowfield; domain widths of several wing spans or more are required to minimize unwanted boundary interactions. To meet these conflicting demands, we utilized a stretched grid in both the vertical and cross-stream directions. The runs presented here utilized more than 2 million grid points ($102 \times 109 \times 242$ downstream) for a part of the simulation. As the wake evolved, altering the grid resolution requirements, new grids were employed, for example, to improve the resolution downstream while relaxing it somewhat cross stream. The minimum grid spacings were 0.6 m in the vertical and cross-stream directions early in the wake evolution, and 1.25 m downstream during the vortex-linking and vortex-ring stages. The domain size was $430 \times 500 \times 320$ m. The downstream domain length is approximately twice the length of the periodicity observed in the data at late times.

We employ periodic boundary conditions in all three directions. Effectively, this means that there are neighboring wakes located at twice the distance to the boundary in the vertical and crosswise directions evolving in parallel with our simulated wake. The stretched grid allows us to place the boundaries at sufficient distance to minimize the effect of these image vortices. Periodicity in the vertical is modified by velocity and temperature jumps to permit wind shear and stratification.

The only significant change in the LES code used here from that used for the simulations in LL96 is the addition of a rotational damping term to the determination of the subgrid turbulence length scale. This was done by adding a term allowing the rotational damping to have the same type of influence on the scale as that represented by the stratification damping term in the previous versions of the code. The primary influence of this term is to reduce the diffusion of the vortex cores due to the subgrid turbulent diffusivity as the wake develops. This would have no effect if we had the luxury of resolution much finer than the vortex core size, but it does allow us to relax the resolution some, particularly in the downstream direction.

The rotational damping term was implemented here in precisely the same way as for our concurrent LES studies of tornado dynamics.[11] No modeling parameters within our LES code have been adjusted for the present comparison.

The conditions used for our primary comparison simulation are summarized in Table 2; these represent our best guess at the corresponding conditions for run 8 of the SNIF flight tests. Where possible, we used the conditions as measured onboard the B-737 during the actual flight-test leg. Uncertainty in our initial conditions comes from uncertainties in the exact dynamics of the atmosphere at the particular time and point in space at which the aircraft passes over the lidar site and uncertainties in the state of the wake a few seconds behind the aircraft. Our initial wake distributions were taken from a UNIWAKE[6,7] simulation with the circulation and integrated heat scaled to match the values given in Table 2, which in turn were estimated from the actual flight speed, aircraft weight, and average fuel consumption (0.32 kg/s). The most important aircraft-dependent parameters in the initial distributions are the circulation about the vortices in the rolled-up state, the vortex separation and core radius, and the integrated sensible heat introduced into the wake by the aircraft.

The exact state of the ambient atmosphere is impossible to ascertain. A separate aircraft, the LaRC OV-10, made measurements of the ambient atmospheric wave/turbulent motions in the vicinity of the observed wake during the test operations. Because these ambient motions are assumed to be the major source of perturbations initiating the wake instabilities, their amplitude significantly influences the detailed structure of the wake as the vortices break up. By Fourier analysis of the wind velocities obtained by the OV-10, we estimated the kinetic energy in the wavelengths close to, and less than, those expected to be most efficient in generating the Crow[12] instability. Before starting the wake simulation, we ran a separate simulation to generate an ambient turbulence field. Beginning with the domain dimensions and temperature stratification to be used for the wake decay simulation, we generated random horizontal velocity and temperature perturbations of relatively large magnitude on a uniform grid (10-m spacing). These were interpolated to a finer grid (5-m spacing) and used as initial conditions in a LES. This simulation was run until the turbulence and gravity waves had a chance to adjust to the temperature stratification and had damped to the desired amplitude range determined by the OV-10 data. A nominal temperature stratification typical of the troposphere was used for the comparison because we were unable to obtain a more precise value of stratification during the experiment, apparently because of a calibration problem with the temperature instrument onboard the OV-10.

IV. Comparison with Experimental Data

Three views of the comparison between experimental lidar measurements and our simulation result for case 1 are shown in Figs. 2–4. The wind at flight altitude sets the drift velocity of the wake across the lidar site as the wake evolves over time. The aerosol species being observed by the lidar is not necessarily a conserved species, with the possibility of either growth via condensation or loss by agglomeration or sublimation. The basic behavior of the wake evolution is similar to that given in LL96 for the B-737 wake for nominal cruise conditions. The view of the simulated wake as it might be seen by the fixed lidar site was obtained by sampling the numerical data on a cross-sectional plane that moves downstream

Table 2 Case 1: initial simulation conditions

Aircraft parameters					
Weight, kg	Airspeed, m/s	Vortex separation, m	Core radius, m	$\int \Delta T \, dy \, dz$, K · m^2	Circulation, m^2/s
40,900	126	22.3	2.5	275	161
Atmospheric conditions					
Altitude, m	Windspeed, m/s	Temperature, °C	Pressure, mbar	N, s^{-1}	Turbulent kinetic energy, (m/s)^2
3,200	7.62	−4	715	0.012	0.002

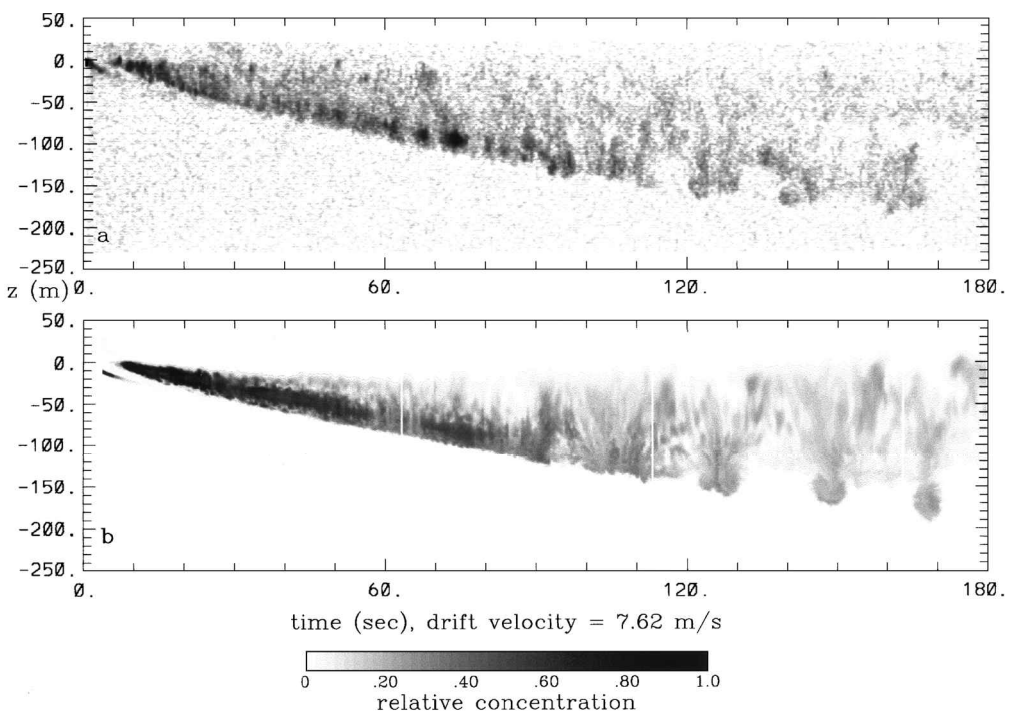

Fig. 2 Time height plot of the instantaneous concentration distribution in the wake behind a B-737 as the wake drifts over a fixed lidar beam: a) experimental results from fixed zenith lidar observations of the engine exhaust aerosol for run 8 on 3/13/96 and b) case 1 simulation results for a conserved tracer added to engine exhausts for our best guess of conditions during the flight.

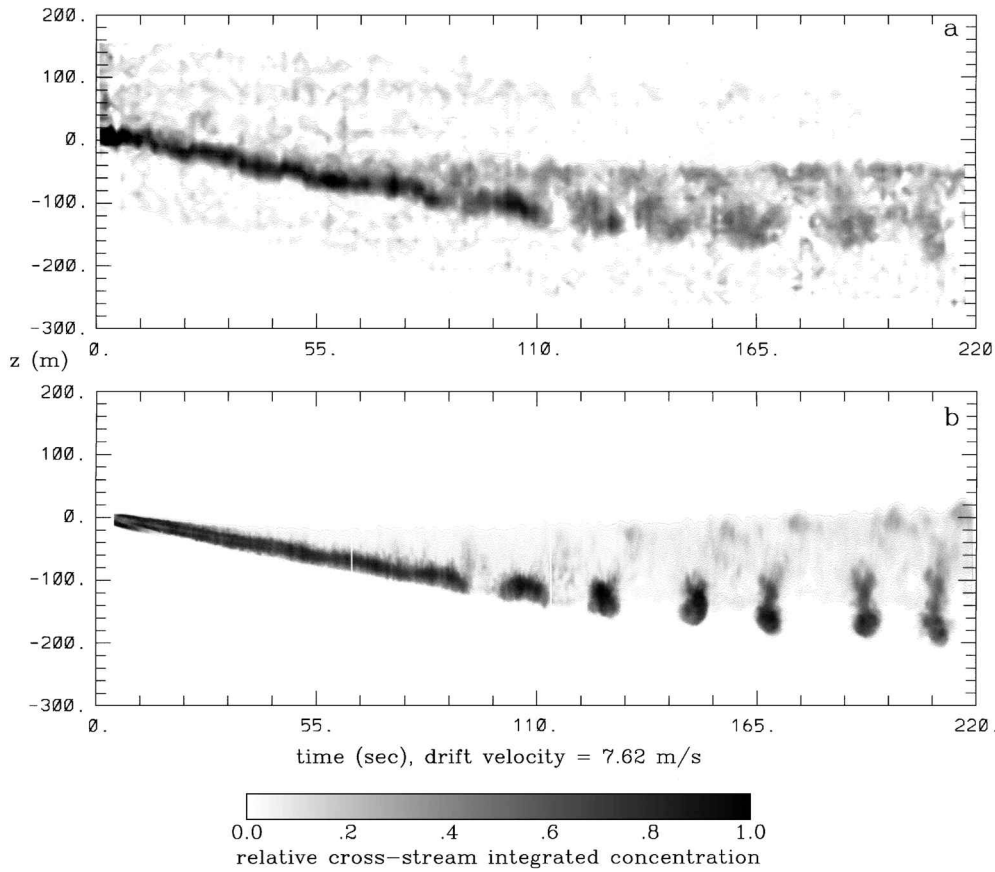

Fig. 3 Time height plot of cross-stream integration of concentration distribution in the wake behind a B-737 as the wake drifts over the observation point: a) experimental results from scanning lidar observations of engine exhaust aerosol for run 8 on 3/13/96 and b) case 1 simulation results for a conserved tracer added to engine exhausts for our best guess of conditions during the flight.

with the prescribed windspeed. This permits the sampling of the LES in essentially the same way as the lidar was sampling the observed drifting wake and provides a convenient representation of the evolution of the periodic Crow structures in both time and space on a single plot.

Figure 2a shows experimental relative enhancement data from the 48-in. zenith-pointing lidar for run 8 at 20:07 EST on 3/13/96 as a function of wake age (in seconds). As these data were collected, the wake drifted over the lidar at a rate of 7.6 m/s. The cross-stream position of the laser beam with respect to the wake is unknown because this position is determined by small misalignments of the wake with the local wind direction. Figure 2b shows the model results for a conserved tracer added to the engine emissions for our best guess at the initial conditions at the time of the test. The vertical slice is taken midway between the initial position of one of the vortex cores and the aircraft centerline. The details of the wrapping of the engine exhausts and the detrainment above the sinking vortices vary depending on the alignment of the drift line with respect to the position of the vortices. In the simulation the tracer initially is distributed uniformly in the downstream direction when the simulation is begun (at a wake age of 4 s); the actual engine exhaust plumes show some clumpiness because of jet turbulence at this early time, giving rise to some of the small-scale variations in the wake seen in Fig. 2a. Figure 3a shows the cross-stream integration of the signals from the ARB scanning lidar. Efforts have been made to display only the relative backscatter from exhaust particulates by subtracting from the signal an estimate of the background atmospheric return. The model results for a conserved tracer are shown in Fig. 3b in the same format as the data. Figures 4a and 4b show the vertical integration of the same scanning lidar results and model results used for the horizontal integration in Fig. 3. Figure 4c shows the vertically integrated pressure deficit in the simulation, which serves as a useful measure of vortex strength and position during the wake evolution.

The vortex-pair wake regime, where the wake sinks at a relatively constant rate because of the mutual interaction of the vortices, is clearly evident in both the measurements and model results. At a wake age of approximately 100 s, the wake develops strong downstream periodicity from the linking of the vortex pair forced by the mutual induction instability. The breakup time of the vortex pair is uncertain to a level of approximately ± 10 s because the position of the wake drifting in the wind is uncorrelated with the time history of the linking process itself. Given the observed wavelength of approximately 160 m and drift velocity of 7.6 m/s, a time difference of 10 s corresponds to a phase difference of one-half a wavelength. The vortex rings formed in this linking process continue to descend, leading to the distinct periodicity evident from approximately 2 min to the end of the observations in Figs. 2–4. The descent of the vortex rings is stopped at about 3 min by a combination of the vortex rings being eroded by small-scale turbulence, the positive buoyancy inherited from the engine exhausts, and the buildup of the buoyancy in the ring as it descends in the stratified atmosphere. Both the measurements and the model results show detrainment of the tracer from the vortex pair in the first minute, with this detrainment significantly increased during the linking process. The positively buoyant plume parcels released during the linking process rise fairly rapidly and are apparent in both the experimental and model results in Fig. 3 as increased concentrations located near the top of the wake plume and situated between the ring puffs in the downstream direction.

The comparison also shows similar overall vertical and horizontal extents of the wake at the end of the observations with these largely determined by the vortex ring dynamics. The apparent vertical spread is a little more for the model than for the observations, with the difference less in Fig. 2 than in Fig. 3, but probably as good as can be expected given the uncertainties involved. The biggest unknown in the model determination of the plume extent is the uncertainty in the local ambient dynamics. There is also some uncertainty in the observed vertical extent inferred from Figs. 2a and 3a because, in the former case, we cannot be sure whether the zenith-pointing lidar beam cuts through the deepest part of the wake plume and, in the latter case, the signal to background measured in the

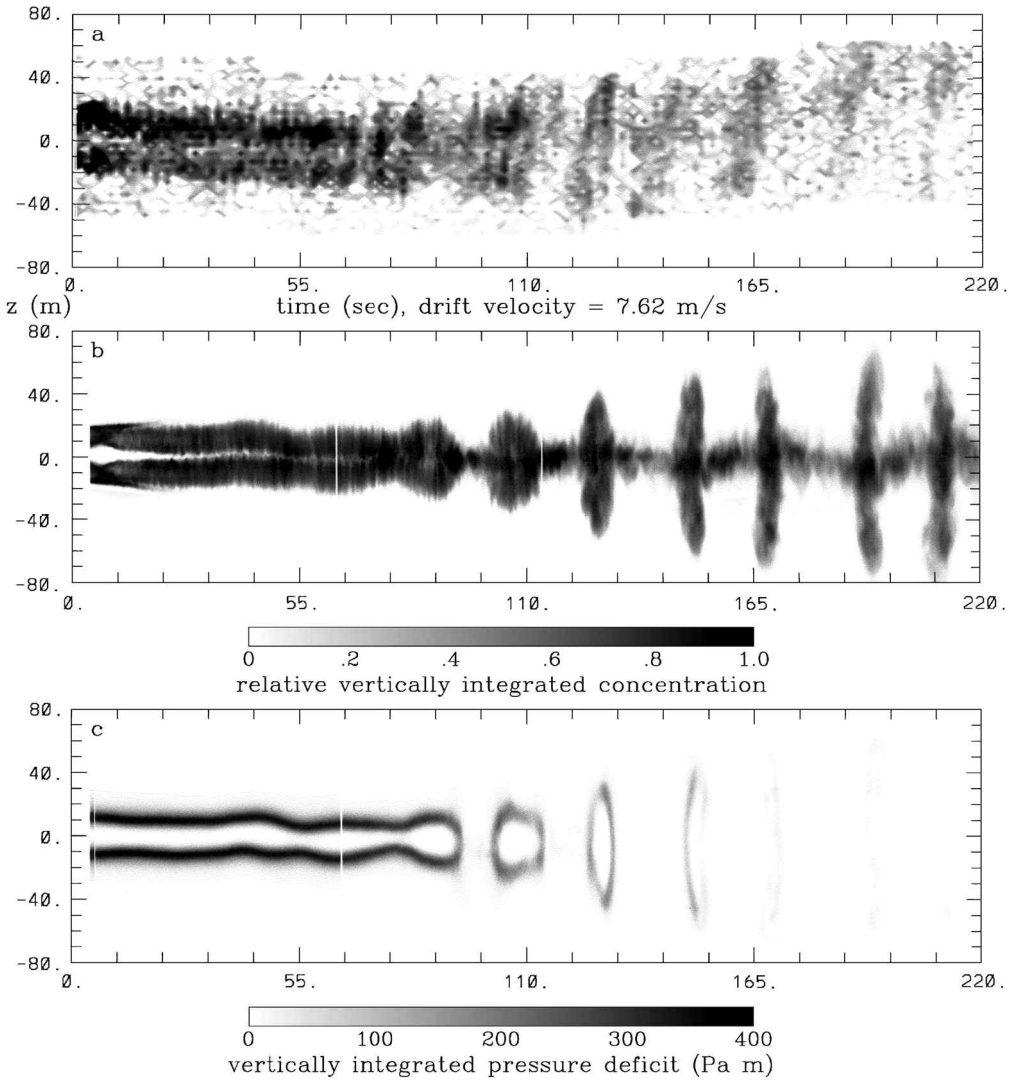

Fig. 4 Time width plot of vertical integration of concentration distribution in the wake behind a B-737 as the wake drifts over the observation point: a) experimental results from scanning lidar observations of the engine exhaust aerosol for run 8 on 3/13/96, b) case 1 simulation results for a conserved tracer added to engine exhausts, and c) simulation results for integrated pressure deficit.

late wake is lower and there is some uncertainty in the background subtraction. The appearance of sharper concentration peaks in the vortex rings seen in Fig. 3b as compared to Fig. 3a is largely due to the alignment of the horizontal integration used to produce these figures. In the experimental data the ring puffs are tilted slightly in the downstream direction, as seen in Fig. 4a, presumably because of a small local ambient wind shear, whereas the simulated ring puffs seen in Fig. 4b are aligned precisely normal to the main wake axis. There is some indication that the scanning lidar may have missed some of the horizontal spread of the wake near the end of the run. It is clear in comparing Figs. 4a and 4b to Fig. 4c that the exhaust tracer concentration distribution serves as only a rough signature of the vortex dynamics during and after vortex linking. Strong vortex rings remain well after the exhaust tracer has been scrambled into less distinct blobs.

The uncertainty in the background signal levels and local atmospheric conditions probably prevents any more quantitative comparison between simulation and observation. Judging from observations of airplane contrails, we expect variations of order 10–20% in the vertical and horizontal extent of different ring puffs in a given wake, even for relatively calm atmospheric conditions. The accuracy of our numerical simulations is difficult to assess with any great precision, given this level of inherent variability as well as the large number of different elements involved in the model. We can get some measure of these uncertainties, however, by degrading some elements of the simulation and noting the effects. We performed a simulation with the case 1 conditions, but with the downstream box size reduced by a factor of 2, and another with the initial velocity distributions from UNIWAKE replaced by ones derived from Gaussian vorticity distributions, with the core size, vortex separation, and circulation as in Table 2. Both simulations give results entirely consistent with those presented here (at the 10% level). In another simulation, the grid resolution was significantly degraded, with the finest grid spacing increased from 0.6 to 1 m and the overall number of grid points reduced by about a factor of 3. In this case the maximum vertical extent dropped by less than 10%, the maximum horizontal extent by 20%, and there was somewhat more early detrainment of the engine exhausts into the upper-wake plume. If used in place of the higher-resolution results of Fig. 2, the qualitative agreement with the experimental results would, if anything, appear to be slightly improved. Finally, we performed simulations with ambient temperature stratification of 0.001 and 0.01 K/m, i.e., significantly below and above the typical tropospheric value of 0.003 K/m that we used in case 1. At late times, relative to the Brunt–Vaisala period, the change in results due to the difference in stratification is readily apparent; however, at the 220-s point (the maximum extent of the lidar data) the differences are minor. The vertical extent of the wake at this time is increased by less than 10% for the lower value of stratification and decreased by 15% for the larger value. The horizontal extents at this time all agree at the 10% level.

Of the 18 flight legs flown parallel to the wind on March 13, 1996, for which the lidars collected data, we chose the one at 20:07

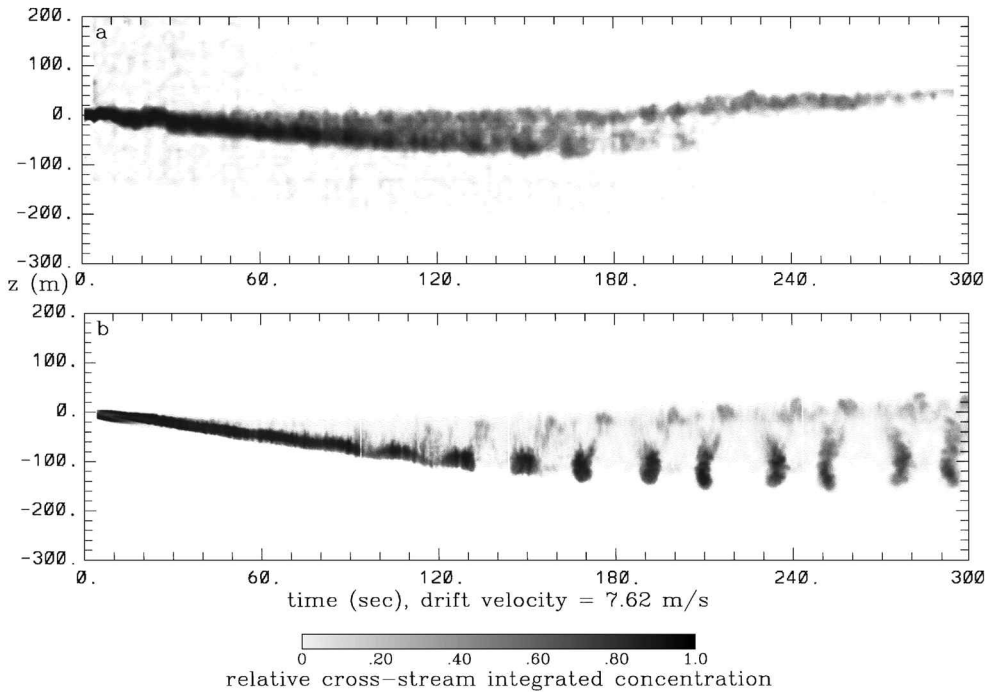

Fig. 5 Time height plot of cross-stream integration of concentration distribution in the wake behind a B-737 as the wake drifts over the observation point: a) experimental results from scanning lidar observations of engine exhaust aerosol for run 21 on 3/13/96 and b) case 2 simulation results for a conserved tracer added to engine exhausts.

EST for our primary comparison with a model simulation because the data set for it was the most complete. In particular, the zenith lidar beam remained in the wake for 3 min during this flight leg, whereas for most others the wake drifted away from the vertically pointing beam relatively quickly; on only one other flight leg did the zenith lidar remain within the wake for more than 2 min. The chosen flight leg had the additional advantage that very little wind shear was in evidence. The data from other flight legs, where available, nonetheless show the same qualitative features that are in evidence in Figs. 2a, 3a, and 4a.

The last six flight legs were flown with a higher airspeed of 184 m/s, such as we consider now in our case 2. For this simulation we used the same initial conditions as for case 1 in Table 2 but with the circulation and integrated engine heat scaled down to 110 m^2/s and 188 K/m^2, respectively, reflecting the higher airspeed. This ignores the reduction in aircraft weight of about 10% between the early- and late-time flight legs due to fuel consumption, as well as the change in rate of fuel consumption associated with the change in airspeed. A comparison of the cross-stream integration of concentration for case 2 with the integrated scanning lidar signal from run 21 at 21:48 EST is shown in Fig. 5. Note that the vortex pair descends somewhat more slowly in the first minute of this simulation than for case 1 (Fig. 3) because of the lower circulation of the vortex pair. This also causes the vortex linking and breakup to proceed at a slower pace, as is evident from both the experimental observations and the model simulation. The breakup wavelength, which depends primarily on the vortex separation and the atmospheric forcing, is roughly the same for both case 1 and case 2. The remnants of the vortex rings are lost in the observations after 3.5–4 min. An inspection of the vertical integration for this case (not shown) indicates the presence of a varying crosswind (and probably some shear), forcing part of the wake out of the scanning volume toward the end of this run.

V. Concluding Remarks

The good qualitative agreement between the experimental observations and the simulated results in Figs. 2–4 demonstrates that the same basic mechanism is acting to break up the trailing vortices in both cases and that the maximum vertical and horizontal extents of the engine exhaust plume is determined largely by these vortex dynamics. There is clear evidence of similarities in the vortex descent rate, vortex breakup, and response to changes in airspeed between cases 1 and 2, in the experimental observations and the simulated results. The vortex-linking timescale, ring extent, dynamics, and lifetime all show good qualitative agreement. The wavelength of the linking agrees but is strongly constrained because an integral number of periods must fit in our periodic downstream domain, the dimension of which was chosen to be consistent with the observed periodicity. The agreement between simulation and experiment is aided considerably by the relatively calm atmospheric conditions at the time of the experiment. This allows the vortex dynamics, for which we have a good handle on the initial conditions within our domain, to dominate the more random atmospheric eddies, whose initial distribution within the experimental domain is unknown to us.

The largest variations between the observations and the simulated results are in the linking and the detrained part of the wake. There are a lot of reasons for variations between individual realizations in both the experimental observations and the simulations. The atmosphere has velocity and temperature fluctuations on a wide range of wavelengths. The smaller scales influence the diffusion of the vortex cores, and the larger scales can affect the local wind shear and stratification. Even when the general atmospheric conditions are reasonably well matched, there will be variations in how the wake interacts with the sum of these fluctuations at a particular point in time and space. This is quite evident in the run-to-run variations observed in the experiments for nominally similar conditions. The simulations show somewhat less variability because there is no energy permitted in wavelengths larger than those permitted in the periodic computational domain but, even here, starting with a different realization of the same turbulent kinetic energy leads to variations in detrainment and the linking process.

Acknowledgments

The simulation work was supported by NASA Grant NAG 1 1635 with W. L. Grose as Technical Monitor. The NASA Langley Research Center Aerosol Research Branch acknowledges the support received from the Flight Operations Support Division and the Transport Systems Research Vehicle and OV-10 ground and flight crews.

References

[1]Friedl, R. R. (ed.), "Atmospheric Effects of Subsonic Aircraft: Interim Assessment Report of the Advanced Subsonic Technology Program," NASA Ref. Pub. 1400, Goddard Space Flight Center, Greenbelt, MD, May 1997.

[2]Schumann, U., and Wurzel, D. (eds.), "Impact of Emissions from Aircraft and Spacecraft upon the Atmosphere," DLR, German Aerospace Reserch Establishment Deutsche Forschungsanstalt fur Luft und Raumfahrt, DLR-Meiteillung 94-06, Cologne, Germany, May 1994.

[3]Spalart, P. R., "Airplane Trailing Vortices," *Annual Review of Fluid Mechanics*, Vol. 30, 1998, pp. 107–138.

[4]Lewellen, D. C., and Lewellen, W. S., "Large-Eddy Simulations of the Vortex-Pair Breakup in Aircraft Wakes," *AIAA Journal*, Vol. 34, No. 11, 1996, pp. 2337–2345.

[5]Gerz, T., Durbeck, T., and Konopka, P., "Transport and Effective Diffusion of Aircraft Emissions," *Journal of Geophysical Research* (submitted for publication).

[6]Quackenbush, T. R., Teske, M. E., and Bilanin, A. J., "Computation of Wake/Exhaust Mixing Downstream of Advanced Transport Aircraft," AIAA Paper 93-2944, July 1993.

[7]Quackenbush, T. R., Teske, M. E., and Bilanin, A. J., "Dynamics of Exhaust Plume Entrainment in Aircraft Vortex Wakes," AIAA Paper 96-0747, Jan. 1996.

[8]DeCoursey, R. M., Poole, L. R., Hostetler, C. A., Kent, G. S., and Hansen, G., "Aircraft Exhaust Particle Measurement with Multiple Ground-Based Lidar Systems," *Proceedings of the Society of Photo-Optical Instrumentation Engineers (SPIE)*, Vol. 3065, Aug. 1997, pp. 9–20.

[9]Sykes, R. I., Lewellen, W. S., and Henn, D. S., "Numerical Simulation of the Boundary Layer Eddy Structure During the Cold-Air Outbreak of GALE IOP-2," *Monthly Weather Review*, Vol. 118, No. 2, 1990, pp. 363–374.

[10]Lewellen, D. C., Lewellen, W. S., and Yoh, S., "Influence of Bowen Ratio on Boundary Layer Cloud Structure," *Journal of the Atmospheric Sciences*, Vol. 53, No. 1, 1996, pp. 175–187.

[11]Lewellen, D. C., Lewellen, W. S., and Xia, J., "The Influence of a Local Swirl Ratio on Tornado Intensification Near the Surface," *Journal of the Atmospheric Sciences* (submitted for publication).

[12]Crow, S. C., "Stability Theory for a Pair of Trailing Vortices," *AIAA Journal*, Vol. 8, No. 12, 1970, pp. 2172–2179.

A. Plotkin
Associate Editor